Modeling Stress Development during the Solidification of Gray Iron Castings

JEFFREY W. WIESE and JONATHAN A. DANTZIG

A method has been developed to predict stress development in gray iron foundry castings. A new yield function, based on theoretical developments by Frishmuth and McLaughlin,[9] and on experiments by Coffin[10] was implemented as a user-written element in a commercial finite element package. The yield function takes into account the strong dependence of the yield stress in cast irons on the loading path. Stresses resulting from thermal displacements in the cooling casting are computed using the new yield function in an elastic-viscoplastic stress analysis. In earlier work, techniques were developed to represent the mold in the thermal analysis by sets of boundary conditions on the surface of the part. For this work, a second user-written element was used to apply force-displacement boundary conditions on the surface of the casting to represent the mechanical constraint of the mold. The properties for this element were based on soil mechanics considerations. Example problems are given, showing a substantial difference in the computed stresses when using the present formulation, in comparison to results obtained with the more usual von Mises yield function.

I. INTRODUCTION

In general, the design of a new cast part is still accomplished through the time-honored method of hand-drawn blueprints, prototyping, and redesign. In order to reduce the expense of this approach, it is desirable to design and evaluate new products on the computer rather than go directly to prototype development. Part of this evaluation involves simulating the heat transfer and thermal stress evolution as the casting solidifies and cools.

Methods for obtaining the thermal history were the subject of previous work by the present authors[1–4] as well as many other researchers.[5] In our work, techniques were developed to eliminate solution of the heat transfer problem in the mold by applying instead a set of boundary conditions to the surface of the casting. These boundary conditions were selected by comparing the local part geometry to those precalculated and stored in a library of candidate boundary conditions. A similar approach was taken for the stress problem: a new boundary condition element was developed to provide the mechanical restraints normally exerted by the mold, eliminating the need to enmesh the mold itself.

When computing the stresses associated with the casting process, proper account must be taken for the mechanical behavior of cast iron.[6] Because the microstructure of gray iron consists of a matrix of steel containing flakes of graphite, the material has very different properties in tension than it does in compression. Under compression, the flakes are held tightly closed, and the bulk material acts very much like steel, though somewhat weaker. Under tension, the flakes bear almost no load, reducing the effective load-bearing area and sometimes acting as stress concentrators. Figure 1 shows the room-temperature tension and compression properties for a typical gray cast iron. In this case, the ratio of compressive strength to tensile strength is approximately 2:1, but it is often greater and could be as high as 5:1.[6] This paper describes a proper representation for the yield surface of gray iron and methods for its incorporation into a finite element analysis. The formulation was incorporated in a commercial code, ANSYS.[7,8]

JEFFREY W. WIESE, formerly at the University of Illinois, is Process Engineer with Reynolds Metals Company, Richmond, VA 23261. JONATHAN A. DANTZIG, Associate Professor, is with the Department of Mechanical and Industrial Engineering, University of Illinois, Urbana, IL 61801.

Manuscript submitted April 26, 1989.

II. METHODS AND RESULTS

A. *Cast Iron Plasticity Element*

In 1976, Frishmuth and McLaughlin examined the failure of cast irons by performing a limit analysis on a "representative volume element" of cast iron.[9] For gray cast iron, the representative volume element was a single eutectic cell, idealized as a cube with cracks (or slits) radiating from the center. The matrix material was assumed to follow the von Mises yield condition, and the slits were assumed to be rough and to have a very small distance between their faces. Thus, any slit which had a net normal tensile force across its face could transmit no stress. A slit which was under compression, though, could transmit both normal and shear stresses. To determine the failure surface, the principal stresses were taken to be normal to the faces. Such behavior produces different behavior in different portions of stress space, depending on the signs of the principal stresses.

The four domains to consider when dealing with a three-dimensional stress state are: the one with three tensile stresses (TTT), the three with two tensile and one compressive stress (TTC), the three with one tensile and two compressive stresses (TCC), and finally the one having three compressive stresses (CCC). Frishmuth and McLaughlin were able to derive mathematical expressions for the failure surfaces in each of these domains. In the following equations, i, j, and k are cyclically permuted from 1 to 3, and tensile stresses are taken to be

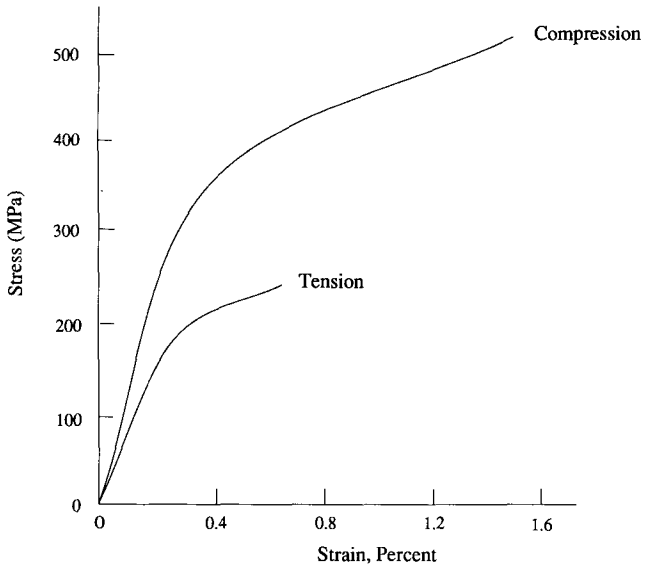

Fig. 1—Room-temperature stress-strain curves for a typical cast iron.[5]

positive. The term σ_i is the average stress in any principal direction in the representative volume element and is defined as

$$\sigma_i = A_m \sigma_i^{\text{bulk}} \quad [1]$$

where A_m is the normalized representative volume element face area minus the projected area of all the slits onto a representative volume element face. Thus, A_m is a dimensionless ratio of the area of slits or, in our case, flakes in the microstructure. The term σ_m is the yield stress for the matrix material (steel).

For the pure tention (TTT) domain, they found the failure surface to be represented by

$$\sigma_i^2 - \sigma_i\sigma_j + \sigma_j^2 = (A_m\sigma_m)^2 \quad [2]$$

For the TTC domain, there were three possible surfaces, given by

$$\left(\frac{\sigma_i}{A_m} - \frac{\sigma_j}{A_m}\right)^2 + \left(\frac{\sigma_j}{A_m} + \sigma_k\right)^2 - \left(\sigma_k - \frac{\sigma_i}{A_m}\right)^2 = 2\sigma_m^2 \quad [3]$$

$$\left(\frac{\sigma_j}{A_m}\right)^2 - \frac{\sigma_j\sigma_k}{A_m} + \sigma_k^2 = \sigma_m^2 \quad [4]$$

$$\sigma_k^2 - \frac{\sigma_k\sigma_i}{A_m} + \left(\frac{\sigma_i}{A_m}\right)^2 = \sigma_m^2 \quad [5]$$

and it was assumed that the innermost (*i.e.*, that corresponding to the lowest stress) was applicable in any particular load case. For the TCC domain, the equation of the failure surface was

$$\left(\frac{\sigma_i}{A_m} - \sigma_j\right)^2 + (\sigma_j - \sigma_k)^2 + \left(\sigma_k - \frac{\sigma_i}{A_m}\right)^2 = 2\sigma_m^2 \quad [6]$$

and for the pure compression (CCC) domain,

$$(\sigma_1 - \sigma_2)^2 + (\sigma_2 - \sigma_3)^2 + (\sigma_3 - \sigma_1)^2 = 2\sigma_m^2 \quad [7]$$

Note that this last equation is the von Mises condition, corresponding to a cylinder about the (1, 1, 1) vector in principal stress space.

Frishmuth and McLaughlin's[9] failure surface incorporates a required feature for the cast iron yield surface: it allows a ratio between failure stresses in compression and in tension to be greater than 2:1. It does this by altering the failure surface shape based on hydrostatic pressure. A yield surface can be formed from the failure surface by noting that it is common practice when working with cast iron to assume that yielding occurs at 25 pct of the ultimate strength.[6] The yield surface was thus obtained by scaling the failure surface to approximately 25 pct of its former size, assuming that the yield point under all loading conditions is proportional to the failure point under those same conditions. This produced a yield surface with a shape geometrically similar to the failure surface. It will be shown that this yield function, with slight modification, compares very well to experimentally determined yielding behavior in multiaxial loading tests. It should be noted that the more commonly used yield surface proposed by Tresca[16] cannot allow a ratio of yield stress in compression to yield stress in tension to be greater than 2:1, so that some new yield function was needed to describe the behavior of cast irons.

The mathematical forms used by Frishmuth and McLaughlin[9] are not convenient for fitting to the experimentally determined properties usually available. For this reason, the equations for the different portions of the yield surface proposed here were rewritten in forms which simplified fitting the yield surface to experimental data, while closely maintaining the shape determined by Frishmuth and McLaughlin. In each case, the new equations were written in terms of the yield for the cast iron in compression, σ_{yc}, and the yield in tension, σ_{yt}, which can be obtained in uniaxial compression or tension experiments. This is as opposed to writing the equations in terms of the yield stress for the *matrix* material, σ_m, as done by Frishmuth and McLaughlin. Note that in the following equations, the numerical value for σ_{yc} should always be negative.

In the TTT octant of three-dimensional principal stress space, the yield surface is a cube (Figure 2(a)), and the equation for the surface has the form

$$\sigma_i = \sigma_{yt} \quad [8]$$

where $i = 1, 2, 3$. In the TCC octants, a paraboloid of revolution was used to join the low yield in tension to the high yield in compression (Figure 2(b)). This surface has the form

$$(\sigma_1^2 + \sigma_2^2 + \sigma_3^2) - (\sigma_1\sigma_2 + \sigma_2\sigma_3 + \sigma_1\sigma_3) - (\sigma_{yc} - \sigma_{yt})(\sigma_1 + \sigma_2 + \sigma_3) = -\sigma_{yc}\sigma_{yt} \quad [9]$$

Within the TTC octants, the yield surface was generated so as to smoothly join the square edge at the side adjacent to the TTT octant (Eq. [8]) with the parabolic shape on the edge adjacent to the TCC octant (Eq. [9]). To generate these portions of the surface, a weighting function (described below) was used which both approximated Frishmuth and McLaughlin's surface and interpolated between the bounding octants to form the surfaces shown in Figure 2(c). Figure 2(d) shows the TTC octant bounded by the axes σ_1, σ_2, and σ_3, along with symbols to describe the generation of the surface. The load point is marked P, and the vector formed by

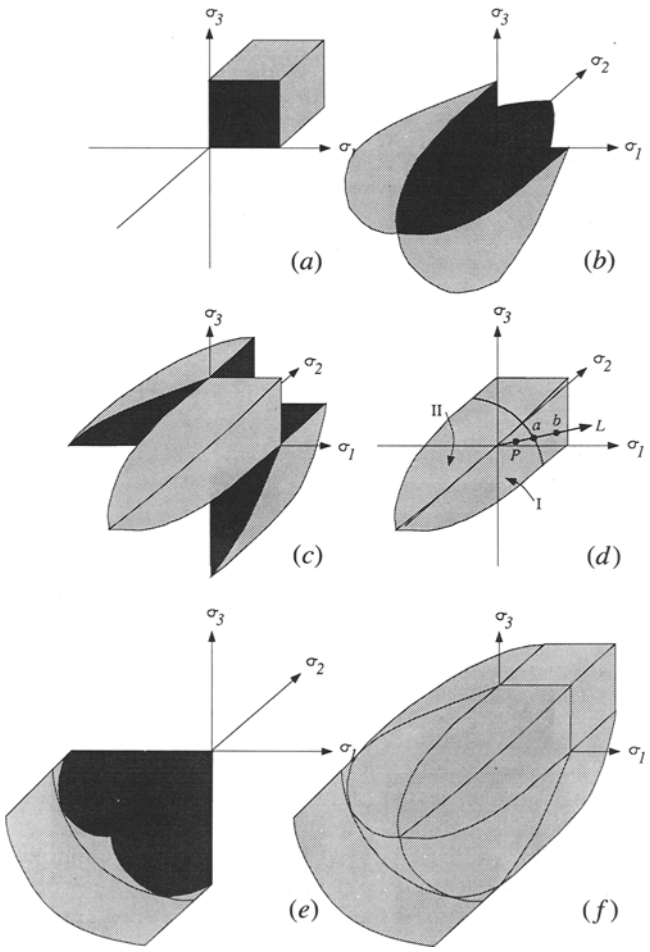

Fig. 2—New yield surface for cast irons. Tension (positive) ends of the stress axes are marked with the stress component labels. (*a*) the TTT octant; (*b*) the three TCC octants; the shape is a paraboloid of revolution; (*c*) the TTC octants; various points used in the interpolation of the yield surface in the TTC octants; regions (I) and (II) are separated by a plane at equal angles to the σ_1 and σ_3 axes; (*d*) the three TTC regions; the shape is interpolated between the paraboloid of the TCC regions and the cube of the TTT octant; (*e*) the CCC region, consisting of a truncated paraboloid of revolution (upper part) and a circular cylinder (lower, von Mises); and (*f*) the assembled new yield surface. Axes correspond to the three principal stress directions.

connecting the origin to *P* is marked **L**. The point at which the vector pierces the paraboloid is called *a*, and *b* is used to denote the point at which **L** pierces the extension of the TTT cube. The boundaries of the paraboloid are marked by dashed lines, and the octant is divided into two portions, marked (I) and (II), by a plane which is at equal angles to the σ_1 and σ_3 planes.

Using this construction, the coordinates for the yield surface in the TTC octant are interpolated between the TTT and TCC values *via*

$$\sigma_i = W_1\sigma_{ia} + W_2\sigma_{ib} \qquad [10]$$

where *i* is cyclically permuted through 1, 2, 3; W_1 and W_2 are weighting factors; and σ_{ia} and σ_{ib} are coordinates for points *a* and *b*, respectively. The weighting factors used are slightly different in regions (I) and (II). In both cases, the factors are based on the angle between one of the axes and a projection of the load vector. The term W_1 is defined as $2\theta/\pi$ and W_2 as $1 - W_1$. In region (I), θ is the angle between the σ_3 axis and the projection of the load vector onto the σ_2-σ_3 plane. In region (II), it is the angle between the σ_1 axis and the projection of **L** onto the σ_1-σ_2 plane. The other TTC regions are treated in a similar manner, and all the TTC regions are shown in Figure 2(c).

In the CCC octant, one of two functions was used, either the paraboloid described above (Eq. [9]) or the von Mises function. Figure 2(e) shows the yield surface in the CCC region. The paraboloid was used when the hydrostatic pressure exceeded

$$\frac{2}{3}(\sigma_{yc} + \sigma_{yt}) - \frac{2}{3}\sqrt{\sigma_{yc}^2 + \sigma_{yc}\sigma_{yt} + \sigma_{yt}^2} \qquad [11]$$

At lower values of the hydrostatic pressure, the von Mises yield criterion was used, having the form

$$(\sigma_1 - \sigma_2)^2 + (\sigma_2 - \sigma_3)^2 + (\sigma_3 - \sigma_1)^2 = 2\sigma_A^2 \qquad [12]$$

where σ_A is the equivalent stress computed in the normal manner at the hydrostatic pressure mentioned above. The von Mises yield function is used in the pure compression region where the cast iron behaves much like steel.

Figure 2(f) illustrates the assembled yield surface. The shape is similar to that obtained by Frishmuth and McLaughlin.[9] By writing the various surface functions in terms of the yield values in tension and compression, any gray cast iron can be represented by simply changing those values. Because of the way the functions are written, however, the absolute value of the yield in compression must always be greater than the yield in tension. This condition is satisfied for all of the irons for which we have found data.

Although not explicitly mentioned above, there is a different yield surface for every temperature as well. It was assumed that the yield functions at different temperatures were geometrically similar, and the parameterization of the yield surface by σ_{yc} and σ_{yt} allowed the use of relatively little input data to fully characterize the material. The yield values at five temperatures were entered, and yield surfaces at intermediate temperatures were obtained by linear interpolation between the input values.

The yield surface is used in the analysis to apportion strain between elastic and plastic deformation. This is done by constructing an "apparent" stress-strain curve *in the direction of the load vector*, with the yield point being the intersection of the load vector with the yield surface at the average temperature of the element under consideration. The method for constructing the apparent stress-strain curve varies with the principal stress octant.

Stress-strain curves for load vectors not parallel to principal stress directions must be constructed by interpolating or extrapolating the uniaxial stress-strain curves, depending on which octant the load vector occupies. The plastic modulus was assumed to be the same in all octants. In the TTT domain, as the hydrostatic pressure increases, the material yields at successively lower stress levels. This corresponds to moving closer to the corner of the TTT cube farthest from the origin. The stress-strain curve was constructed by translating the plastic portion of the pure tension curve down along the elastic portion until the yield point matched that required by the

yield surface (Figure 3). By the same token, for most of the CCC domain, the yield point exceeds that found in the uniaxial compression test. In this case, the plastic portion of the pure compression curve is translated upward along the elastic line until the yield is in accordance with the yield surface.

In the TTC and TCC domains, the curve must lie somewhere between the uniaxial tension and uniaxial compression curves. The yield point computed from the yield surface was used as a weighting factor to interpolate between the tension and compression curves. The value for the interpolated stress at any particular strain in these octants was

$$\sigma_i = \frac{(\sigma_{ys} - \sigma_{yt})(\sigma_c - \sigma_t)}{(\sigma_{yc} - \sigma_{yt})} + \sigma_t \qquad [13]$$

where σ_i = the interpolated stress at a particular strain;
σ_c = the stress from the compression curve at a given strain;
σ_t = the stress from the tension curve at a given strain;
σ_{ys} = the yield stress computed from the yield surface;
σ_{yc} = the yield stress from the compression curve; and
σ_{yt} = the yield stress from the tension curve.

As a result of this procedure, the interpolated curve has a shape that is intermediate between the tension and compression curves.

The new yield surface compares well to experimental data. Biaxial stress states may be achieved experimentally using tubular test specimens, with forces directed along the axis and internal pressure applied to provide hoop stresses. Figure 4 shows the new yield surface along with data presented by Coffin.[10] The points in the compression-compression quadrant were obtained by applying pressure to the outside of the tubular specimen.

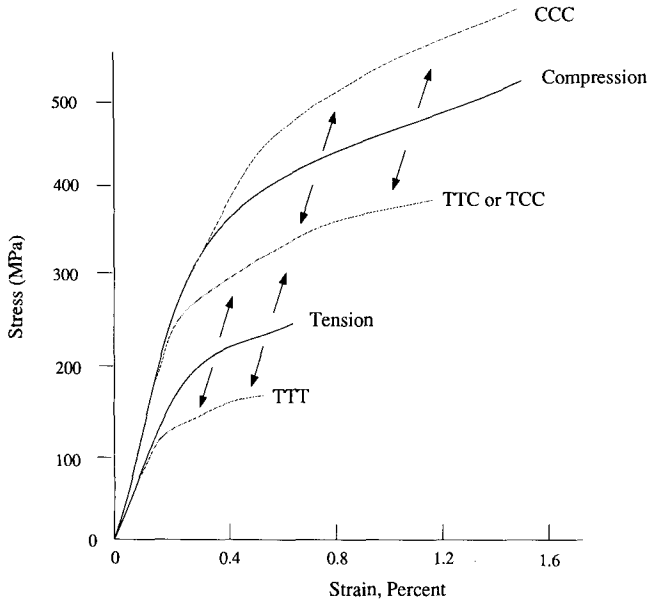

Fig. 3—Interpolation and/or extrapolation to determine the effective stress-strain curve in the various portions of principal stress space.

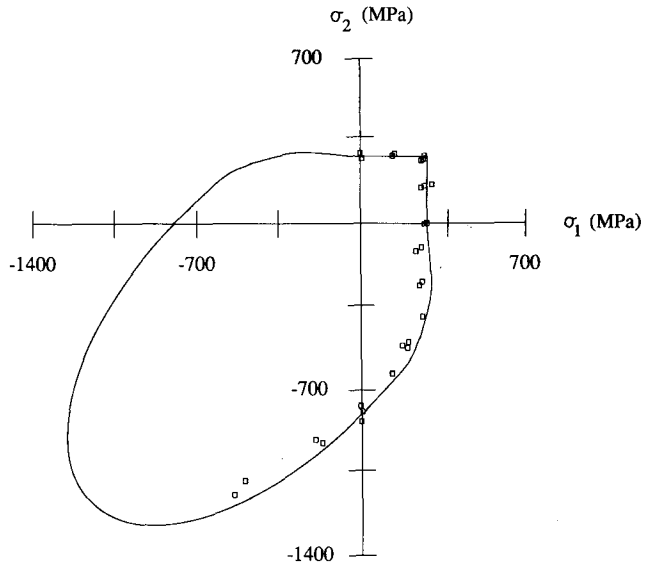

Fig. 4—New yield surface compared to data obtained in biaxial tension-torsion experiments by Coffin.[10]

The agreement between the yield surface and experimental data is good and can be improved in most cases by slightly altering the yield points in tension and compression used to construct the yield surface.

In Figure 4, it can be seen that there are small areas at the intersections of the surface with the positive axes where the yield surface is concave. This condition is not strictly legal,[11] but both the areas and the magnitudes of the concavity are small. The equations describing the surface would be much more complicated if the concavities were eliminated, and the concavity appeared not to affect the results significantly.

The code necessary to implement the new yield surface was inserted into ANSYS at the point it normally does the property interpolation based upon temperature. The added code, when activated, performs both the temperature interpolation and the interpolation based on the yield surface and loading path described above. The effect is to pass back to ANSYS both an "apparent" stress-strain curve and a plastic strain increment based on the new yield surface. The capacity to model creep behavior was unaffected by the alterations, so that viscous behavior could also be included in simulations.

Because ANSYS uses the initial stress method,[7] iteration must be performed at each load step to obtain a solution. When using the new yield function, the mechanical properties depend on both the stress state and the temperature, which can cause them to vary greatly from one iteration to the next. This effect was found to be somewhat detrimental to convergence, requiring more load steps and more iterations than were needed when using the von Mises yield surface. Comparisons of results using both methods are described in Section II–C.

B. *Boundary Condition Element*

In the Introduction, it was pointed out that for computational efficiency, the mold itself was not modeled, and so a special element was required to apply the mechanical boundary conditions corresponding to deformation of the mold. In an actual casting, as the metal

pushes against the sand mold, it will be resisted by compression of the sand. As the sand is compressed, however, it also crushes so that it does not return to its former position if the casting later moves away.

Such behavior can be represented by a two-noded finite element with three components, shown schematically in Figure 5: a spring to provide the resisting force as the sand is compressed, a gap which allows the casting to move away from the mold without being hindered, and a ratchet to provide for the crushing of the sand. As the mold is compressed, the ratchet sets at successively larger displacements. Later, as the casting moves away, the ratchet portion remains set at its previous displacement, and the casting recedes with no resistance. If the casting were to later come into contact with the mold, the resisting force would resume at the level it attained when the element was previously compressed.

As in the case of the yielding behavior of the iron, the sand behavior was implemented in ANSYS by altering an existing element.[8] The original element (STIF7) consisted of a spring and gap in series, thus containing two of the three components mentioned above. It had two nodes which define the direction of the spring force. One node was connected to the casting at one of the elements making up the model, and the other node was usually fixed to a reference point in space.

The ability to model gap formation without spring-back was added to this element by storing the largest negative displacement between the nodes of each boundary element in a separate variable. In subsequent load steps, a resisting force is generated only when the computed negative displacement exceeded the previously stored value. Thus, in the new formulation, the stored values were used as an offset when calculating whether or not the gap was open.

C. *Example Problem*

The example problem comprised the freezing of a dumbbell shape. Symmetry allowed the model to contain only a small portion of the entire geometry. The dumbbell was cut at the center of the handle, and a small slice in the azimuthal direction was taken from the half-geometry. The handle radius was 15 mm, the handle half-length was 50 mm, the head diameter was 65 mm, and the head length was 30 mm (Figure 6).

The composition of the cast iron is listed in Table I,[4] and the thermal properties used are listed in Table II (adapted from Reference 12). The cast iron freezes over the range of 1145 °C to 1136 °C, and the (initial) pouring temperature was 1350 °C. Note that the thermal conductivity (in Table II) at high temperatures was raised to

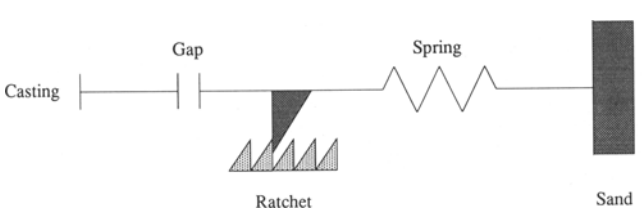

Fig. 5—Schematic representation of new mechanical boundary condition element. Casting is on the left; the right side is fixed.

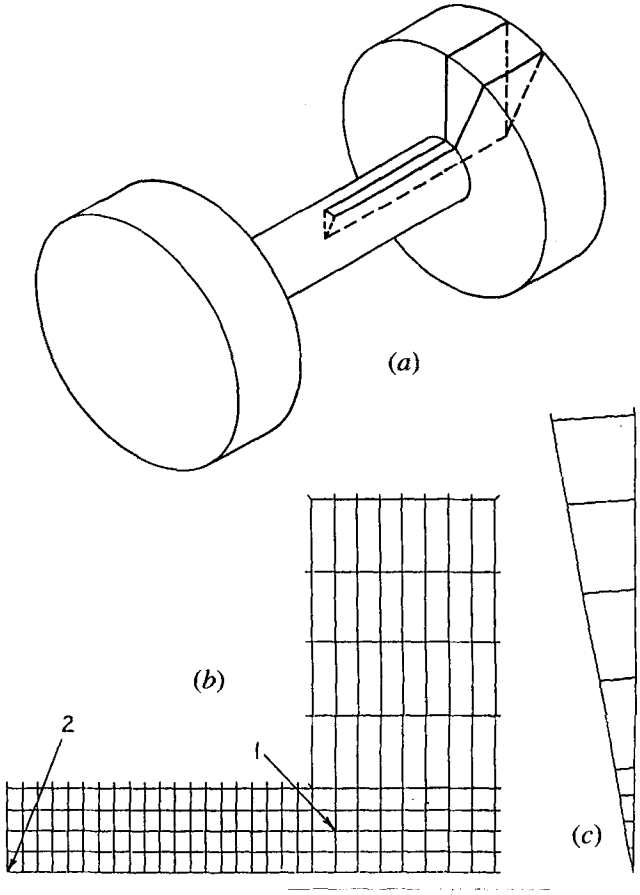

Fig. 6—(*a*) Geometry and (*b*) finite element mesh for the dumbbell example problem. (*c*) The model is one element thick, corresponding to 10 deg.

simulate the effect of convection in the liquid portions of the casting. The thermal expansion coefficients of Table II were derived from the density data. An important point to note from the thermal expansion data of Table II is that there is a volume *increase* associated with falling temperature during the eutectoid transformation (731 °C to 723 °C). This fact can have a profound effect on the stress fields that develop, including a reversal of sign of principal stresses. This moves the material response from one octant to another in principal stress space, greatly changing its behavior.

The geometry and mesh for this example were generated within ANSYS. The thermal analysis is not dependent upon the stress history in this kind of casting, so the thermal and stress analyses were run in sequence. As the thermal analysis ran, the computed temperatures at the various time-steps were written to a binary file (FILE4), and the stress analysis read back the temperature data stored in FILE4 to compute thermal stresses. The time data were used to compute stress relaxation.

Two stress analyses were performed, an elastic-viscoplastic analysis using a von Mises yield surface based on the tensile yield stress and an elastic-viscoplastic analysis utilizing the new yield surface. In both cases, 72 load steps were used, Poisson's ratio was 0.3, and the reference temperature for the thermal expansion coefficients was 1350 °C.

Bilinear approximations were used for the stress-strain

Table I. Composition of Iron Used in the Example Problem

C	S	Si	Cu	Ni	Mn	Cr	P	Al
3.45	0.064	1.33	0.11	0.088	0.42	0.058	0.012	0.003

curves for the von Mises yield surface, and a kinematic hardening rule was applied in both the old and new methods. These properties were adapted from Reference 13. It was found in the stress analysis that at high temperatures, the liquid material had to have some strength for the solutions to converge. As shown in Table III, even at the highest temperature, the cast iron was assumed not to yield until stressed to 1 MPa. The curves were defined for ANSYS by entering a temperature for the curve, a yield stress (the strain is computed from the Young's moduli of Table II), and a tangent modulus (set equal to 25 pct of the Young's modulus). Smaller values for the tangent modulus also created convergence problems. The new modifications to the stress element require input of the stress-strain properties as five curves for the tension domain and five curves for the compression domain, each having five segments and each at a different temperature. These data are shown in Table IV (adapted from Reference 13).

ANSYS has several creep equations available.[7] The primary creep equation chosen for the example problem was (in incremental form)

$$\Delta\varepsilon_{cr} = A\sigma^B t^C e^{-D/T}\,\Delta t \qquad [14]$$

and the secondary creep equation was

$$\Delta\varepsilon_{cr} = E\sigma^F e^{-G/T}\,\Delta t \qquad [15]$$

where σ is the equivalent stress, t is time, e is the base for natural logarithms, and T is the absolute temperature. The values for the constants A through G, shown in Table V, were chosen by referring to Figure 53 of Reference 6 (not included in this paper), which gives the creep behavior of a class 40 cast iron under various stresses and a temperature of 500 °C. Variation of creep behavior with temperature (the values for constants D and G) was taken to be the same as that of 304 stainless steel.[14]

The spring stiffness for this model was assumed to be 1000 MPa, corresponding to the stiffness of the cast iron just after solidification. This stiffness was multiplied by the area associated with each surface node to determine a unique spring force for each boundary condition element. This number was an estimate, based on the ultimate strength for foundry sands.[6,15] The displacements normal to the symmetry surfaces of the dumbbell model were set to zero.

Especially with three-dimensional models, the issue of how to present the results of an analysis arises. One method of collapsing the stress state of any point down to one number is to plot a stress ratio based on the principal stresses. In the following figures, the stresses are represented as a ratio between a principal stress and a yield stress. For each element, the two quantities σ_1/σ_{yt} and σ_3/σ_{yc} are formed, where σ_1 is the first (maximum tensile) principal stress, σ_3 is the magnitude of the minimum principal stress (compressive stress with greatest magnitude), σ_{yt} is the yield stress in tension at the current temperature, and σ_{yc} is the magnitude of the yield stress in compression at the current temperature. In all cases, the maximum of the two quantities is plotted, rather than any particular stress component.

Figures 7(a) and (b) show the results of the analyses for times of 560 and 1440 seconds, corresponding to states just after solidification and immediately after the eutectoid transformation, respectively. In each case, window 1 shows the temperature, window 2 shows the stresses computed using the new yield surface, and window 3 shows the corresponding stresses using the von Mises yield surface. Figures 8 and 9 compare computed stress ratio histories at two locations in the dumbbell, computed using the two yield functions. The figures clearly show that the maximum stress ratios achieved, and the times at which they were reached, were very different when using the two methods. The computing times (Sun 3/280 with floating point accelerator (FPA)) for the different phases of the analysis were 6320 seconds for the thermal analysis, 46,290 for the old method (included a restart, so time was greater than necessary), and 36,406 for the new method.

III. DISCUSSION

In window 2 of Figure 7(a), the analysis using the new yield surface, there are two areas with a stress ratio above 3.0. These points would be very likely to fail in an actual

Table II. Thermal Properties of the Cast Iron Used in the Example Problem

Temp. (°C)	c_p (J/g K)	$\bar{\alpha}$ (1/°C)	Temp. (°C)	k (W/mm K)	Temp. (°C)	ρ (kg/mm^3)	Temp. (°C)	E (MPa)
25.0	0.540	1.525×10^{-5}	27.0	0.07693	25.0	7.220×10^{-3}	25.0	1.96×10^{4}
723.0	0.732	1.753×10^{-5}	328.0	0.04566	599.4	7.053×10^{-3}	200.0	1.72×10^{4}
723.5	10.860*	1.755×10^{-5}	717.0	0.03530	694.4	7.077×10^{-3}	657.0	6.00×10^{3}
731.5	10.860*	2.231×10^{-5}	1135.0	0.02000	794.4	7.034×10^{-3}	815.0	3.00×10^{3}
732.0	0.6400	2.232×10^{-5}	1140.0	0.01400	911.3	7.006×10^{-3}	1136.0	1.00×10^{3}
1136.0	0.7000	2.922×10^{-5}	1250.0	0.01680	1144.4	6.923×10^{-3}	—	—
1136.5	31.10	4.929×10^{-5}	1300.0	0.02716	1155.8	6.995×10^{-3}	—	—
1144.5	31.10	1.00×10^{-10}	1350.0	0.09240	1177.5	6.960×10^{-3}	—	—
1145.0	0.9175	—	1375.0	0.18900	1199.2	6.919×10^{-3}	—	—
1400.0	0.9073	—	1400.0	0.28000	1349.6	6.800×10^{-3}	—	—

*Heat of transformation taken from 1086 steel in Reference 12.

Table III. Mechanical Properties Used for the Stress Analysis with Von Mises Yield Function

Temperature (°C)	Yield Stress (MPa)	Tangent Modulus (MPa)
25.0	49.0	4900.0
200.0	43.0	4300.0
675.0	12.0	1500.0
815.0	3.0	750.0
1136.0	1.0	250.0

Table V. Creep Constants Used in the Simulations

Constant	Value
A	6.294×10^{-4} MPa^{-B} s^{-C-1}
B	1.5
C	−0.6
D	5000 K
E	6.124×10^{-8} MPa^{-F} s^{-1}
F	2.0
G	5000 K

casting. On the other hand, in window 3, corresponding to the analysis using the von Mises yield function, no stress ratio exceeds about 1.5, a perfectly acceptable level of stress. These results are important because it is at high temperatures that hot tears occur, and including a more physically representative model for the material behavior results in a completely different conclusion about the manufacturability of the designed part.

At a later time (Figure 7(b)), the computed stress ratios are actually lower when using the new method, although neither method predicts stress ratios that are unduly large. This reversal in stress levels is due to the fact that the higher stresses and greater strength in compression allowed in the new method analysis produced more plastic and creep flow in the shaft at high temperatures. Later, as the temperatures fell, less stress developed in the shaft because of its slightly greater length. At times greater than 1440 seconds, the stresses once again became higher for the new method, but the difference between the two methods was small.

The time dependence of the stress development, shown in Figures 8 and 9, also merits some discussion. Point 1 is in the high-stress area near the handle-head joint (Figure 8), and point 2 is on the axis at the center of the handle, another high-stress area. During the eutectoid transformation (approximately 960 to 1440 seconds) and immediately after, the old method stress ratios are larger than the new method values, as discussed above. At the time of shaking out from the mold (2560 seconds), the stresses are again higher for the new method. Note that the stresses at this point are those which exist in the casting prior to its removal from the mold. To determine the residual stresses outside the mold, the spring constants for all the mechanical boundary elements would be reduced to zero, and the temperature would be allowed to fall to ambient levels.

Two other dumbbell analyses were run, though the results are not presented here. One used a simple spring element to apply the mechanical boundary conditions, and the other used the new boundary condition element but with a sand stiffness of only 500 rather than 1000 MPa. The first run, using the simple spring boundary conditions, gave stress results that were virtually identical to the run using the new boundary condition element. This was encouraging, because the gap components of the active elements, those on the inside faces of the dumbbell head, stayed closed for the most part. Thus, the behavior of the important boundary condition elements should have been, and was, very much like that of simple spring elements.

The results of the second run, with a sand stiffness of 500 MPa, were surprising at first, since these stresses were also very much like the stresses of the 1000 MPa case. It was realized, however, that both 500 and 1000 MPa are probably stiffer than most foundry sands. In both cases, the stress state in the casting was pushed

Table IV. Mechanical Properties Used for the Stress Analysis with New Yield Function

Tension Curves									
25 °C		200 °C		675 °C		815 °C		1136 °C	
Strain (Pct)	Stress (MPa)	Strain (Pct)	Stress (MPa)	Strain (Pct)	Stress (MPa)	Strain (Pct)	Stress (MPa)	Strain (Pct)	Stress (MPa)
0.25	49.00	0.25	43.00	0.20	12.00	0.10	3.00	0.10	1.00
0.91	95.05	0.91	83.41	0.73	23.28	0.36	5.82	0.36	1.94
2.74	127.3	2.74	111.7	2.19	31.18	1.10	7.80	1.10	2.60
6.06	138.6	6.06	121.7	4.85	33.95	2.43	8.49	2.43	2.83
1.13	142.2	1.13	124.8	9.03	34.83	4.51	8.71	4.51	2.90
Compression Curves									
25 °C		200 °C		675 °C		815 °C		1136 °C	
Strain (Pct)	Stress (MPa)	Strain (Pct)	Stress (MPa)	Strain (Pct)	Stress (MPa)	Strain (Pct)	Stress (MPa)	Strain (Pct)	Stress (MPa)
0.75	147.0	0.75	129.0	0.60	36.00	0.30	9.00	0.30	3.00
1.90	232.0	1.90	203.6	1.52	56.82	0.76	14.21	0.76	4.74
4.15	302.9	4.15	265.8	3.32	74.19	1.66	18.55	1.66	6.18
7.63	357.6	7.63	313.8	6.10	87.57	3.05	21.89	3.05	7.30
14.18	407.6	14.18	357.7	11.34	99.81	5.67	24.95	5.67	8.32

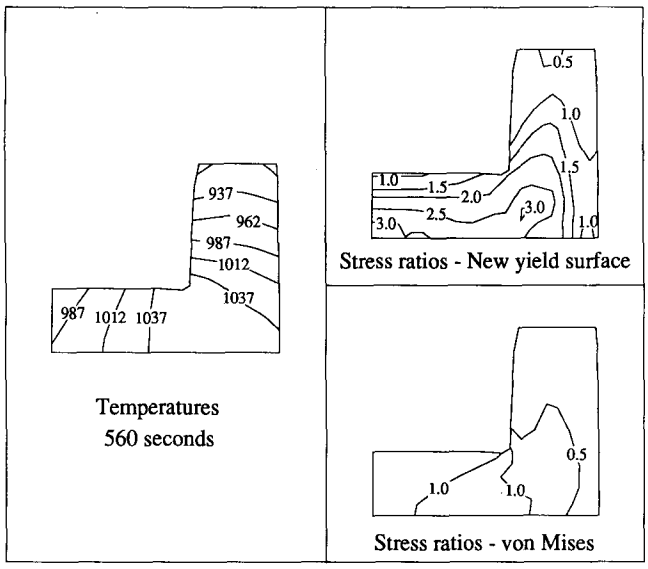

(*a*)

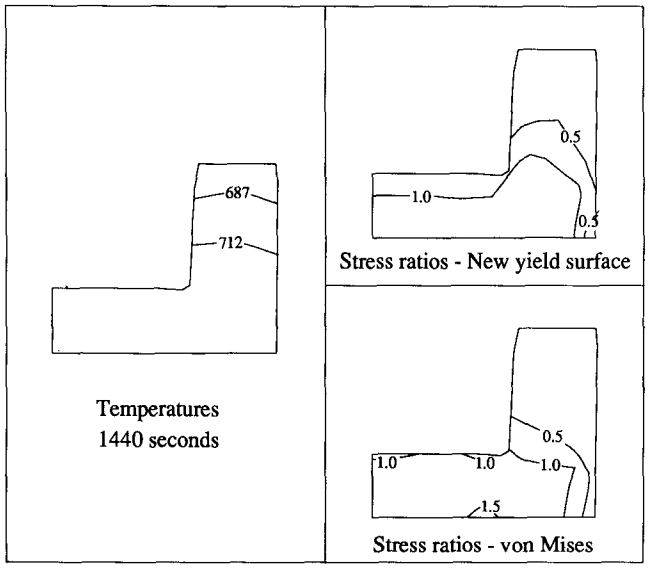

(*b*)

Fig. 7—Thermal and elastic-viscoplastic stress results for the dumbbell-shaped example problem. Window 1 shows temperatures (legend is above right). Window 2 shows new method stress ratios, and window 3 shows old method stress ratios. (*a*) Solution 560 s after pouring (just after solidification) and (*b*) solution 1440 s after pouring (immediately after the eutectoid transformation).

up onto the flat portion of the stress-strain curve. Under those circumstances, stresses could be relieved through plastic strain without causing the buildup of additional stress.

It would be ideal if experimental results were available to compare to these stress computations. Unfortunately, little detailed residual stress data exist for cast iron. One reason for this is the simple fact that it is very difficult and expensive to measure residual stresses with any degree of accuracy. X-ray methods yield good results, but only for a very thin layer of material at the surface.

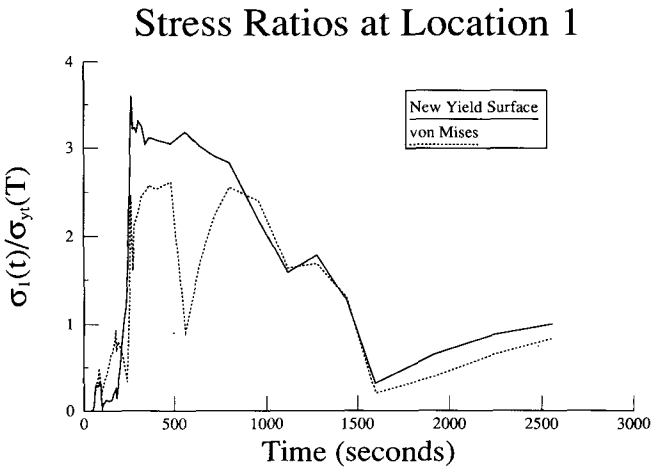

Fig. 8—Time histories of maximum computed tensile principal stress divided by yield stress at location 1 in the model, using two different yield functions.

Methods are available which involve placing strain gages on the surface and drilling a hole to relieve stresses. The displacements measured by the gages can then be related to the stresses that existed before the hole was drilled, provided the stress-strain relationship is accurately known. Another possibility is to place strain gages around the area of interest and then to physically cut the object. Again, the strains can be related to the original residual stresses with a known stress-strain relation. These last two methods involve averaging of the residual stresses over somewhat indeterminate volumes, while the first method examines a very small portion of the object. Both extremes make it difficult to match the measurements to the finite element predictions.

An approach that is being taken at Deere and Company, Moline, IL, is to design a casting with a relatively simple geometry which lends itself to the specific purpose of measuring residual stresses. The casting consists of a ring of rectangular cross section and a cross bar, having the overall shape of the Greek letter theta. The intention

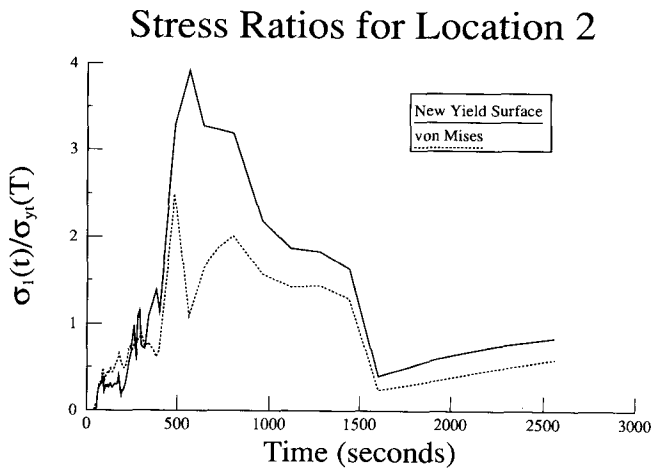

Fig. 9—Time histories of maximum computed tensile principal stress divided by yield stress at location 2 in the model, using two different yield functions.

is that the ring will cool much faster than the bar at the center and yield plastically. When the bar later freezes, it will be in tension. The bar can be cut and reference points on its surface measured to yield a displacement which could be related to the average residual stress in the bar.

IV. CONCLUSIONS

Because of its radically different behavior in tension and compression, the stress-strain response of gray cast iron is very difficult to model. A new constitutive model for gray iron, which expands upon previous work and is easily incorporated into any finite element package, was presented.

An example problem was given to compare the computed stresses using the new yield surface to those computed using a von Mises yield surface. Creep deformation was also included. Comparison of the calculations for experimental results would be useful, but no such results are available at this time.

ACKNOWLEDGMENTS

The authors would like to thank Deere and Company Technical Center, Moline, IL, and the University of Illinois Materials Processing Consortium for their support of this work.

REFERENCES

1. J.W. Wiese and J.A. Dantzig: *Appl. Math. Modeling*, 1988, vol. 12, pp. 213-20.
2. J.A. Dantzig and J.W. Wiese: *Adv. Manufacturing Processes*, 1986, vol. 1, pp. 437-54.
3. J.A. Dantzig and S.C. Lu: *Metall. Trans. B*, 1985, vol. 16B, pp. 195-202.
4. J.A. Dantzig and J.W. Wiese: *Metall. Trans. B*, 1985, vol. 16B, pp. 203-09.
5. A.F. Giamei and G.J. Abbaschian: *4th Conf. of Modeling and Control of Casting and Welding Processes*, TMS-AIME, Warrendale, PA, 1988.
6. C.F. Walton and T.J. Opar: *Iron Castings Handbook*, Iron Castings Society, Cleveland, OH, 1981, pp. 203-95.
7. G.J. DeSalvo and J.A. Swanson: *ANSYS Engineering Analysis System User's Manual, Volume I*, Swanson Analysis Systems, Inc., Houston, PA, 1985, pp. 2.27.1-2.27.19.
8. G.J. DeSalvo and J.A. Swanson: *ANSYS Engineering Analysis System User's Manual, Volume I*, Swanson Analysis Systems, Inc., Houston, PA, 1985, pp. 4.7.1-4.7.6.
9. R.E. Frishmuth and P.V. McLaughlin: *J. Mater. Technol.*, 1976, vol. 98, pp. 69-75.
10. J.L.F. Coffin: *J. Appl. Mech.*, 1950, vol. 17, pp. 233-48.
11. D.C. Drucker: *1st U.S. Congress of Applied Mechanics*, 1952, vol. 1, pp. 487-91.
12. R.D. Pehlke, A. Jeyarajan, and H. Wada: *Summary of Thermal Properties for Casting Alloys and Mold Materials*, NTIS-PB83-211003, University of Michigan, Ann Arbor, MI, 1982.
13. M.R. Ozgu: *Thinner Walled Ingot Molds: Mathematical Modeling of Thermal Stresses and Plant Trials With Lighter Big-End-Up Molds*, Inland Steel Presentation, E. Chicago, IN, 1983.
14. G.J. DeSalvo and J.A. Swanson: *ANSYS Engineering Analysis System User's Manual, Volume I*, Swanson Analysis Systems, Inc., Houston, PA, 1985, p. 8.4.
15. R.W. Heine, C.R. Loper, and P.C. Rosenthal: *Principles of Metal Casting*, McGraw-Hill, New York, NY, 1967, pp. 84-122.
16. H. Tresca: *Compt. Rend.*, 1864, vol. 59, p. 754.